Uncovering the Lagrangian Skeleton of Turbulence

Manikandan Mathur,[1] George Haller,[1*] Thomas Peacock,[1]
Jori E. Ruppert–Felsot,[2] Harry L. Swinney.[3]

[1]Department of Mechanical Engineering, MIT
77 Massachusetts Ave., Cambridge, MA 02139, USA
[2]Department of Physics, University of Tokyo
302-304, Faculty of Science Bldg.1, 7-3-1 Hongo, Bunkyo-ku, Tokyo, 113-0033, Japan
[3]Department of Physics, University of Texas at Austin
Austin, Texas 78712, USA
[*]To whom correspondence should be addressed; E-mail: ghaller@mit.edu.

Turbulent transport underlies a vast range of environmental and engineering phenomena, yet its detailed understanding remains elusive. Here we report on a new technique that uncovers the Lagrangian building blocks of turbulence in two-dimensional flow experiments. Combining recent experimental and dynamical systems techniques, we identify an intricate network of attracting and repelling material lines that are responsible for turbulent fluid motion in a rotating flow forced by jets from below. The resulting chaotic tangle, the Lagrangian skeleton of turbulence, shows a striking level of spatio-temporal complexity that has only been observed previously in theoretical and numerical examples of strange attractors. For the first time in an experimental flow, we quantify the strength, or hyperbolicity, of each material line in the skeleton, and demonstrate dramatically different mixing events in different parts of the tangle.

It is now widely recognized that coherent structures emerge even in the most disordered fluid flows. While coherence can sometimes be naturally detected by visual inspection, extracting coherent structures from experimental or numerical flow data has proven to be a challenging task.

One of the difficulties is the lack of a universal definition for coherence in the Eulerian (lab) frame: high or low values of vorticity, pressure, strain, and energy have all been suggested as defining quantities. They all, however, tend to favor different structures, partly because of a lack of unambiguous threshold values over which a flow region is to be considered coherent. More alarmingly, Eulerian indicators of coherence are frame-dependent,[1,2] and hence are often unsuccessful in capturing intrinsic flow properties in unsteady flows.

By contrast, coherent structures in the Lagrangian (particle-based) frame can be defined in a frame-independent way as distinguished sets of fluid particles that have a decisive impact on fluid mixing by their special stability properties.[3−6] Such Lagrangian coherent structures (LCS) are straightforward to envision based on the wealth of literature on chaotic advection[7,8]; it is quite another matter, however, to identify LCS in a finite-time flow data set where stability properties of individual fluid particles are difficult to establish.

Recent experimental work[9] showed that LCS in real-life, time-periodic laminar fluid flows mimic the complicated tangles predicted by numerical studies of chaotic advection in time-periodic flow models. In the time-periodic case, particle image velocimetry (PIV) applied to a relatively small number of particles can provide a highly resolved velocity field. Indeed, taken into account with the proper phase, the same particles yield more and more detail about the periodically repeating velocity field as time progresses[9]. The same approach is inapplicable to turbulent flows for lack of a distinguished period. A further challenge in locating LCS in turbulence is the high noise levels and the dramatically increased spatial complexity, both of which have been absent in LCS studies of time-aperiodic but low-Reynolds-number experi-

mental flows[10]. As we shall see below, the irregular temporal and spatial features of turbulence create LCS of previously unseen complexity, and thus require refined analysis.

In the present work, we combine recent experimental techniques with new LCS detection tools to seek the analogues of laminar chaotic tangles in a nominally two-dimensional turbulent flow. Experiments were conducted on flow in a rapidly rotating tank of water that was $50\ cm$ high and $40\ cm$ in diameter, as described in [11]. This paper concerns the quasi-two-dimensional turbulent flow near the top of the tank, where the Reynolds number was $\mathrm{Re} \approx 1000$ and the Rossby number was $Ro \approx 0.3$ (the tank rotation rate was 4 Hz). Flow in the tank was driven by strong pumping of fluid through an array of small-scale sources and sinks in the bottom of the tank. This produced a strongly turbulent three-dimensional flow with $\mathrm{Re} \approx 6 \times 10^4$ and $Ro \approx 20$ near the tank bottom. With increasing height in the tank, the three-dimensional flow evolved into quasi-two-dimensional turbulence due to the influence of rotation and the decay of the three-dimensional turbulence.

A snapshot of the horizontal velocity field and the corresponding vertical vorticity field measured in a horizontal plane $4\ cm$ below the tank lid are shown in figures 1a and 1b . The flow contains many long-lived coherent vortices and jets with a wide range of sizes. The measurements were made using Digital Particle Image Velocimetry (DPIV) with neutrally buoyant tracer particles illuminated by a horizontal laser light-sheet.[11] A CCD camera (1004×1004 pixels resolution, 30 frames per second) captured images of the particles, which were densely seeded in the flow. The laser was strobed to obtain successive images more closely separated in time than the frame rate by straddling neighboring frames. A digital particle image velocimetry algorithm called Correlation Image Velocimetry (CIV)[12] was used to obtain snapshots of the instantaneous field from correlations over many small integration regions of pairs of images. Each run yielded a sequence of 300 snapshots separated by $\Delta t = 1/15\ s$ and calculated on a 128×128 spatial grid with 0.3 cm resolution. A detailed description of the measurement

technique and an analysis of errors are given in [11].

The measured vertical vorticity field exhibited complex dynamics such as vortex birth, merger, scattering and destruction. Measurements with a vertical laser light sheet revealed that the coherent structures were columnar and extended vertically throughout the tank. The quasi-two-dimensional flow near the top of the tank is described well by the vertical vorticity field.[11] In Fig. 1c, we show the variation of the magnitude of the integrated divergence along particle paths (zero for a purely two-dimensional flow) over a period of 8 seconds. The scalar quantity, being large in magnitude only in small regions in the entire domain, suggests that the flow is predominantly two-dimensional. A measure of the average factor by which the entire spatial domain gets deformed (spatial average of the exponent of the integrated divergence) over 8 seconds comes out to be 0.994, fairly close to unity, which is the expected value for a two-dimensional flow.

To post-process the experimental velocity field, we use cubic interpolation in space and linear interpolation in time to obtain a refined velocity field on a 600×600 grid with time step $\Delta t = 0.01s$. Using the refined velocity does not improve the detection of Eulerian coherent structures. It will, however, lead to high-resolution LCS detection with resolutions exceeding that of the raw Eulerian data. By the mathematical properties of hyperbolic sets, any LCS whose length scale is well-separated from the refined grid scale is guaranteed to exist in the original flow.[6]

As a first step in understanding the Lagrangian structure of turbulence, we adopt the Lyapunov-exponent-based LCS detection scheme[4] applied previously to laminar-flow experiments with periodic[9] and aperiodic[10] time dependence. Specifically, we solve numerically for particle trajectories $\mathbf{x}(t, \mathbf{x}_0)$ starting from points $\mathbf{x}_0$ on the refined velocity grid at a fixed initial time t_0. By numerical differentiation, we compute the largest singular-value field $\lambda_{\max}(t, t_0, \mathbf{x}_0)$ of the deformation-gradient tensor field $(\partial \mathbf{x}(t, t_0, \mathbf{x}_0)/\partial \mathbf{x}_0)^T (\partial \mathbf{x}(t, t_0, \mathbf{x}_0)/\partial \mathbf{x}_0)$. We then use the

Direct Lyapunov Exponent (DLE) field $\sigma_{t_0}^{t}(\mathbf{x}_0) = [\log \lambda_{\max}(t, t_0, \mathbf{x}_0)] / (2(t - t_0)$ plotted over initial positions $\mathbf{x}_0$ to visualize LCS.

For $t \gg t_0$, repelling LCS at t_0 can be located as local maximizing curves (i.e., *ridges*) of the $\sigma_{t_0}^{t}(\mathbf{x}_0)$ field.[3–6] Similarly, for $t \ll t_0$, attracting LCS at t_0 can be located as ridges of the $\sigma_{t_0}^{t}(\mathbf{x}_0)$. Detected for evolving initial times t_0 and large enough integration times T, sharp evolving ridges of $\sigma_{t_0}^{t_0+T}(\mathbf{x}_0)$ and $\sigma_{t_0}^{t_0-T}(\mathbf{x}_0)$ turn out to be close to evolving material lines, i.e., the fluid flux across them at any time t_0 is negligible[13]. We note here that the primary topological features of the LCS extracted from the DLE field are not sensitive to the integration time T. However, small values for T result in very weak ridges and longer integration times reveal more details of the ridges. We choose T = 8 seconds in our analysis so that the scalar field can be visualized easily and also that the primary features of the LCS show up as strong visually-obvious ridges in the appropriate scalar fields.

We show a typical result of the DLE calculation in Fig. 2a. The zoomed-in portion shown in Fig. 2b suggests underlying large-scale topological ridges for the DLE field, but due to the high level of turbulent noise, these large-scale ridges are disguised by peaks and valleys whose size is of the order of the grid size. The unavoidable noise comes partly from measurement uncertainties, but also partly from the sensitive nature of fluid trajectories in a turbulent flow. As a result of this sensitivity, nearby particles will end up at very different locations due to inevitable errors in their numerical advection. Corresponding to these different locations, significantly different DLE values arise in our computations. We therefore need new computational tools to extract large-scale DLE ridges reliably from our turbulent flow data.

To this end, we note that for any fixed time t_0 and large enough T, a ridge of the DLE field $\sigma_{t_0}^{t_0+T}(\mathbf{x}_0)$ acts as an attractor for the gradient dynamical system

$$d\mathbf{x}_0/ds = \boldsymbol{\nabla}\sigma_{t_0}^{t_0+T}(\mathbf{x}_0), \tag{1}$$

where s denotes the arclength along the gradient lines of $\sigma_{t_0}^{t_0+T}(\mathbf{x}_0)$ and $\boldsymbol{\nabla}$ denotes the spatial gradient with respect to the initial position $\mathbf{x}_0$. We exploit this attracting property in ridge extraction as follows:

1. For any t_0 and large enough T, fix a narrow region D around the ridges where the magnitude of the gradient $\boldsymbol{\nabla}\sigma_{t_0}^{t_0+T}(\mathbf{x}_0)$ is over a predefined threshold.

2. From the grid points in D, compute numerically, solutions $\mathbf{x}_0(s)$ to the gradient system (1).

3. For each value of s and large enough T, compute the Hessian matrix $\boldsymbol{\nabla}^2\sigma_{t_0}^{t_0+T}(\mathbf{x}_0(s))$; discard points where $\boldsymbol{\nabla}^2\sigma_{t_0}^{t_0+T}(\mathbf{x}_0(s))$ does not have at least one negative eigenvalue, a prerequisite for a ridge.

4. For the remaining points, find the eigenvector $\mathbf{e}_{t_0}^{t_0+T}\left[\mathbf{x}_0(s)\right]$ corresponding to the eigenvalue of $\boldsymbol{\nabla}^2\sigma_{t_0}^{t_0+T}(\mathbf{x}_0(s))$ that is smaller in norm. Stop the computation once the angle between $\mathbf{e}_{t_0}^{t_0+T}\left[\mathbf{x}_0(s)\right]$ and $\boldsymbol{\nabla}\sigma_{t_0}^{t_0+T}(\mathbf{x}_0(s))$ shows no appreciable change. For large enough T, this eigenvector will approximate a tangent vector to a ridge.

Fig. 2a shows ridges (in black) of the backward-time DLE field extracted by the above algorithm at time $t_0 = 9.89$ sec. using $T = 8\ sec.$ We have obtained a similar level level of detail and accuracy for other t_0 values also.

While hyperbolic material lines create DLE ridges, the converse is *not* true: a DLE ridge may simply indicate a material line of high shear that does not attract or repel nearby particles at an exponential rate.[6] For a DLE ridge to be hyperbolic, it must contain a *hyperbolic core* that plays a role analogous to that of saddle points in steady flows. Namely, a truly repelling DLE ridge will act as a stable manifold for a hyperbolic core, while a truly attracting DLE ridge will act as an unstable manifold for a hyperbolic core.

Previous studies of laminar flows did not differentiate between truly hyperbolic material lines and lines of high shear. The ubiquitous presence of shear in a turbulent flow, however, requires such a differentiation, i.e., identification of possible hyperbolic cores along DLE ridges. By recent mathematical results[6], hyperbolic cores can be detected using the rate of strain tensor $\mathbf{S}(\mathbf{x}, t)$, the symmetric part of the velocity gradient field $\boldsymbol{\nabla}\mathbf{v}(\mathbf{x}, t)$. Specifically, if $\mathbf{n}\left(t_0, \mathbf{x}_0\right)$ is a unit normal to a forward-time DLE ridge at the point $\mathbf{x}_0$ at time t_0, then $\mathbf{x}_0$ is contained in a hyperbolic core of a repelling material line if the inner product $\nu_{t_0}\left(\mathbf{x}_0\right) = \left\langle \mathbf{n}\left(t_0, \mathbf{x}_0\right), \mathbf{S}(t_0, \mathbf{x}_0)\mathbf{n}\left(t_0, \mathbf{x}_0\right)\right\rangle$ is positive. Negative values of the same inner product on a backward-time DLE ridge reveal hyperbolic cores of attracting material lines. These statements are backed by mathematical proofs[6], but have not yet been evaluated on experimentally or numerically generated velocity fields.

Figure 3(a) shows the first implementation of the hyperbolicity criterion on our turbulent flow data. The background colour in the image indicates the strength (hyperbolicity) of the attracting material lines in the region. Regions containing strongly attracting material lines are in red and those containing backward-time DLE ridges that are weakly attracting are in white. The ridges from the backward-time DLE field are plotted in blue. We see that almost all DLE ridges in our flow field have hyperbolic cores and hence represent truly hyperbolic material lines. We verify the location of hyperbolic cores by advecting a fluid blob starting near a core, then comparing the blob's deformation to that of other blobs released away from hyperbolic cores. Figures 3b & 3c show two snapshots of the evolution of a black blob released near a hyperbolic core, a blue blob released on an LCS ridge but away from hyperbolic cores, and a purple blob released away from LCS ridges. The dramatic stretching of the black blob compared to the other two blobs confirms the presence of a hyperbolic core, and illustrates that the given LCS ridge is indeed an attracting material line.

The results in Fig. 3b & Fig. 3c justify identification of hyperbolic material lines with the

set of forward-time and backward-time DLE ridges. Shown in Fig. 4, the full set of red ridges are stable manifolds for trajectories in the hyperbolic cores, whereas the set of blue ridges are unstable manifolds for the hyperbolic cores. A general fluid particle is subject to attraction to nearby blue curves and simultaneous repulsion by nearby red curves. The complex tangle formed by these two curves is the underlying cause of turbulent particle motion, the *Lagrangian skeleton of turbulence*. Its complexity is beyond what has been seen for laminar flows. Most notably, the skeleton appears to fill the whole flow domain densely without leaving any unmixed islands. It also appears, that all hyperbolic cores interact with themselves through homoclinic tangles, as well as with any other core through a chain of intersecting heteroclinic tangles. Such behavior has only been observed before in numerical examples of strange attractors, such as the well-known Lorenz attractor.[14]

The analytical and numerical methods employed in this work extend to three-dimensional flows, but the experimental measurement of three-dimensional turbulent velocity fields is not yet within reach. Nevertheless, ongoing work on the direct numerical simulation of three-dimensional turbulent channel flows indicates the existence of a similar Lagrangian skeleton formed by two-dimensional surfaces.

References

1. J. Jeong, F. Hussain, *J. Fluid. Mech.* **285**, 69(1995).

2. G. Haller, *J. Fluid. Mech.* ***525,*** 1(2005).

3. G. Haller, G. Yuan, *Physica D* **147**, 352(2000).

4. G. Haller, *Physica D* **149**, 248(2001).

5. G. Haller, *Phys. Fluids* **13**, 3365(2001).

6. G. Haller, *Phys. Fluids* **14**, 1851(2002).

7. H. Aref, *J. Fluid Mech.* **143**, 1 (1984).

8. J. Ottino, *Ann. Rev. fluid Mech.* **22**, 207 (1990).

9. G. A. Voth, G. Haller, J.P. Gollub, *Phys. Rev. Lett.* **88**, 254501(2002).

10. S.C. Shadden, J.O. Dabiri, J.E. Marsden, *Phys. Fluids* **18**, 047105(2006).

11. Jori E. Ruppert-Felsot, Olivier Praud, Eran Sharon, Harry L. Swinney, *Phys. Rev. E* **72**, 016311(2005).

12. A. Fincham and G. Delerce, *Expt. Fluids* **29** (*Suppl.*): S13(2000).

13. S.C. Shadden, F. Lekien, J.E. Marsden, *Physica D* **212**, 271 (2005).

14. John Guckenheimer, Philip Holmes, *Nonlinear Oscillations, Dynamical Systems, and Bifurcations of Vector Field*s (Springer-Verlag, New York, 1983).

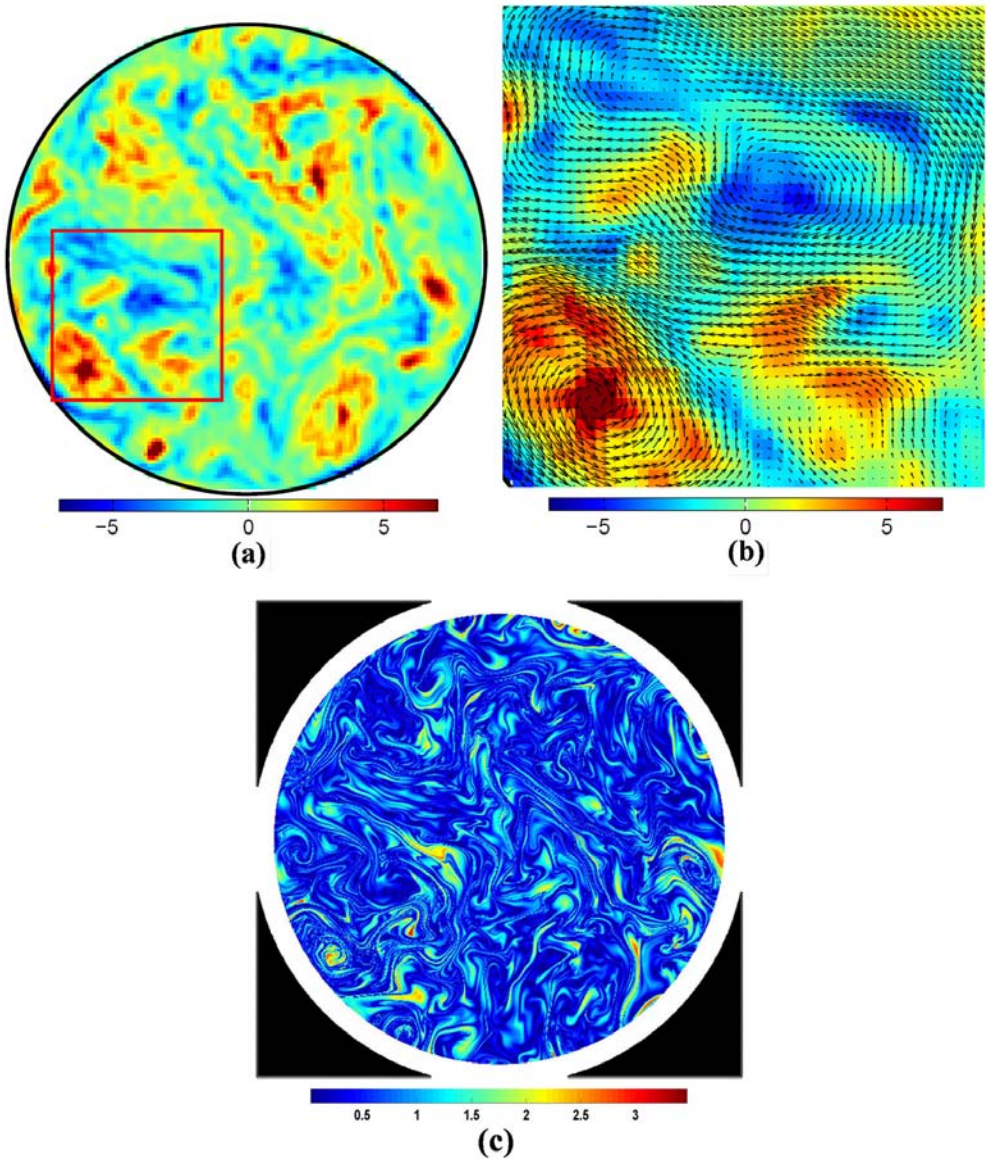

Figure 1: (a) A snapshot of the vertical vorticity field in an experiment on a fluid in a rapidly rotating 40 cm diameter tank. The colorscale is saturated to bring out the weaker features. (b) A close-up of the boxed region in (a) with the velocity field indicated by arrows. The largest velocity if 6.5 cm/s and the largest (smallest) value of vorticity is 12.3 (-5.8) s^{-1}. (c) Absolute value of the integrated divergence (along particle paths) over 8 seconds in forward time. Regions close to the wall are shown in white as the estimates of the divergence field in those regions are inaccurate.

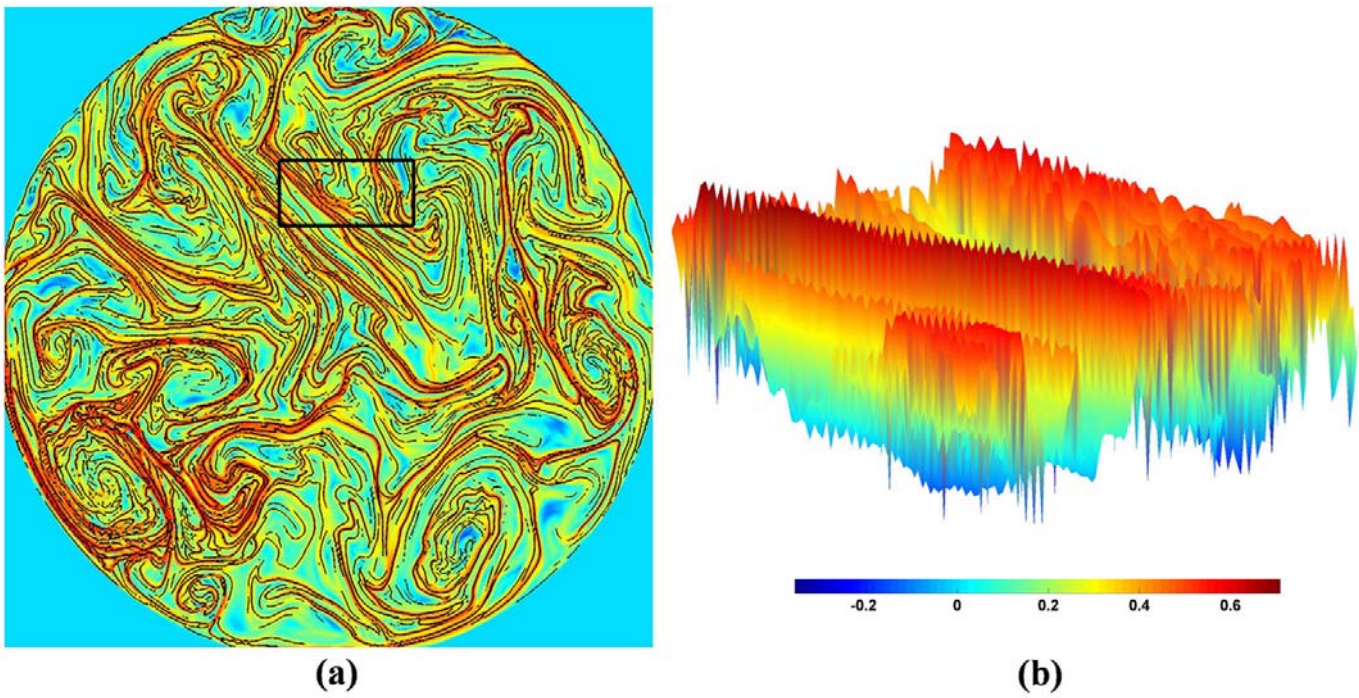

Figure 2: (a) Ridges of the backward-time DLE field (in s^{-1}) at t_0 = 9.89 sec. extracted by gradient climbing and filtering, with T = 8 sec. (b) A closer look at the noise levels in the scalar field over the boxed region in (a).

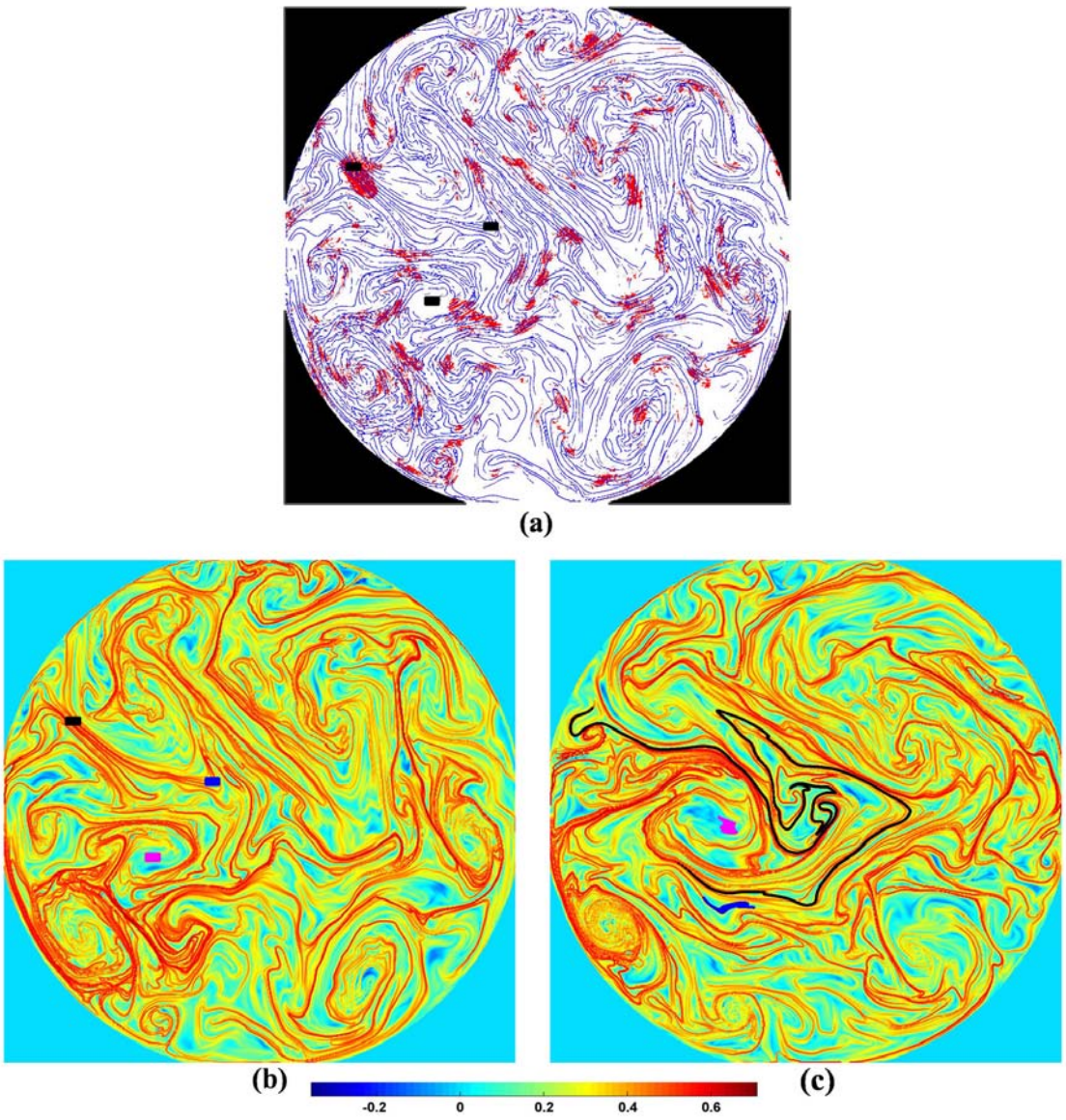

Figure 3: (a) Ridges from the backward-time DLE field at t_0=9.89 sec. The background color indicates how strongly attracting (hyperbolic) the region is. Red color indicates strong attraction and white indicates weak/zero attraction. (b)&(c) Evolution of three fluid blobs with the backward-time DLE field (in s^{-1}) at t_0=9.89 sec and 16.89 sec. The evolution is computed numerically from the experimental velocity field. The initial locations of the blobs are indicated by the black boxes in (a).

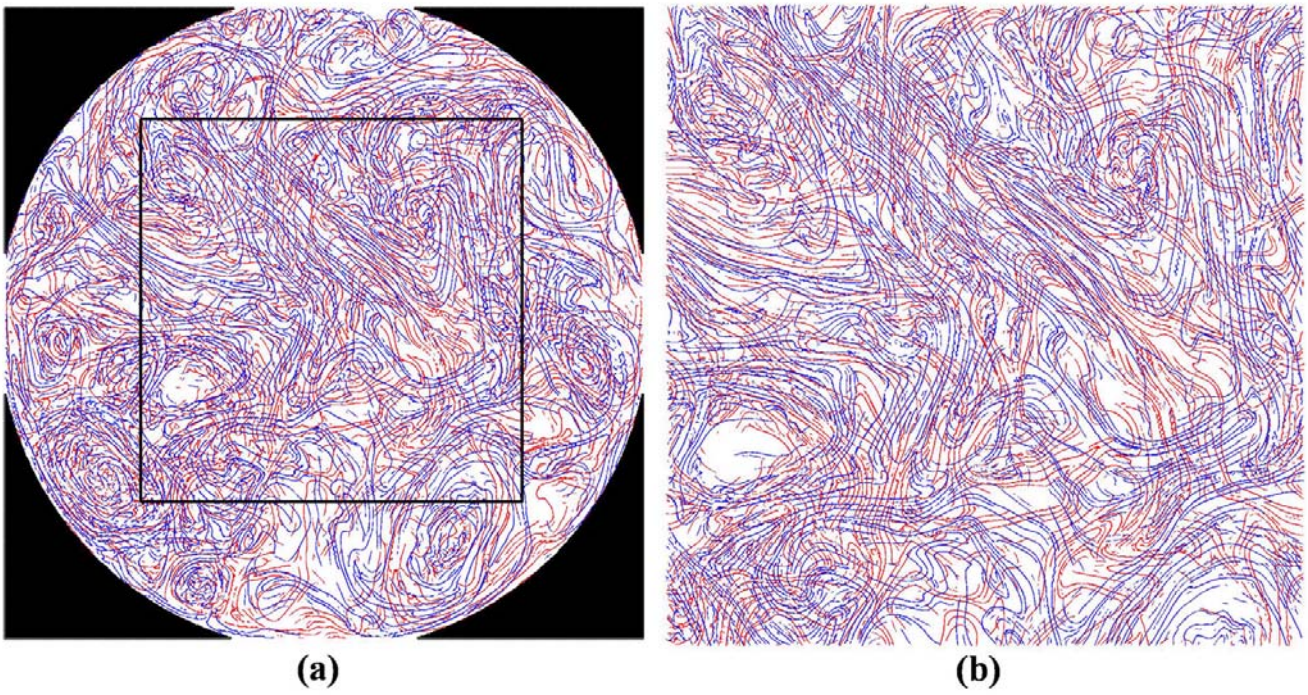

Figure 4: (a) Stable (red) and unstable (blue) manifolds at t_0 = 9.89 sec extracted from the experimental flow data. (b) A close-up of the boxed region in (a). The integration time for evaluating the DLE field is 9.8 seconds in (b) to capture the finer details of the stable and the unstable manifolds.